OPEN ACCESS
IOP Publishing
Journal of Physics G: Nuclear and Particle Physics
J. Phys. G: Nucl. Part. Phys. **47** (2020) 045115 (25pp)
https://doi.org/10.1088/1361-6471/ab67ea

Comparative analysis of the Coulomb barrier in heavy-ion collisions by the double-folding method

O K Ganiev[1] **and A K Nasirov**[1,2]

[1] Institute of Nuclear Physics, Uzbekistan Academy of Science, 100214 Tashkent, Uzbekistan
[2] Joint Institute for Nuclear Research, Dubna, Russia

E-mail: nasirov@jinr.ru

Received 18 September 2019, revised 20 December 2019
Accepted for publication 6 January 2020
Published 9 March 2020

Abstract

The double-folding formalism has been applied to calculate the nucleus-nucleus potential by the use of the effective nucleon-nucleon (Migdal) potential and the nuclear densities of the interacting nuclei presented as the Gaussian-type functions and polynomials. The Coulomb barrier heights obtained by this way and by different types of the proximity potentials have been compared. The deviations of the theoretical values of the Coulomb barrier from the values extracted from the experimental data are discussed. The capture cross section calculated for the reactions with the light projectiles is in good agreement with experimental values. The theoretical results obtained for the $^{16}O+^{144}Sm$ and $^{17}O+^{144}Sm$ reactions could reproduce a significant difference in the experimental results for these reaction, which is related with the extra neutron in ^{17}O. The overestimation of the experimental data obtained from different sources by the curve of the theoretical results of the $^{40}Ca+^{96}Zr$ reactions is explained by the appearance of the slight hindrance to complete fusion, *i.e* the capture and fusion cross sections are not equal in this reaction.

Keywords: double-folding method, nucleus-nucleus potential, Coulomb barrier, capture reaction, nuclear density

(Some figures may appear in colour only in the online journal)

Original content from this work may be used under the terms of the Creative Commons Attribution 4.0 licence. Any further distribution of this work must maintain attribution to the author(s) and the title of the work, journal citation and DOI.

1. Introduction

In nuclear physics, heavy-ion fusion reaction around the Coulomb barrier is one of the most popular topics of research [1–4] due to great interest to study the fusion mechanism of nuclei and its dependence on the entrance channel of the process. The Coulomb barrier of the entrance channel is an important quantity determining the possibility of realization of different reaction channels in the heavy ion collisions at low energies. Currently, numerous theoretical and experimental investigations are being related to systematically study the capture reactions leading to several interesting phenomena, such as the complete fusion, quasifission, incomplete fusion, fast-fission and formation of the evaporation residues which has been used to synthesise the superheavy elements (see for instance [4–19] and references therein). At the analysis of this type of reactions, the nuclear interaction potential plays an important role in determining the fate of the interacting nuclei [1, 20–30]. The total interaction potential of the two interacting nuclei is taken as the sum of the short-range nuclear attractive potential, the long-range Coulomb repulsive potential and rotational energy. The strong competition between the repulsive Coulomb potential and the attractive nuclear interaction at the close distances causes the Coulomb barrier and potential well which determine conditions for the realization of the definite reaction mechanism. The energy of relative motion must overcome this Coulomb barrier in order for the colliding nuclei to be captured and fused. A crucial step in investigating these interactions is the calculation of interaction potential between nuclei that can help us to evaluate the fusion cross-section of various fusion reactions.

Nevertheless, different theoretical models depending on the vast variety of assumptions have been developed to analyze the experimental values of the Coulomb barrier: for example, different versions of the proximity potential [20, 31–35], the Bass model [22, 36–38], the Christensen and Winther potential [39], the Broglia and Winther potential [23, 40], the Akyüz-Winther potential [41, 42], and the Woods–Saxon potential [43], the Skyrme energy density formalism [44] and the double-folding [45] etc. Among such theoretical approaches, the double-folding potential calculated by the integration of the nucleon densities of the interacting nuclei with the effective density-dependent nucleon-nucleon (NN) interaction, which is widely used in describing the heavy-ion fusion reactions.

The Coulomb barrier height can be determined from the barrier distribution extracted from the fusion (capture) excitation function. In order to obtain the Coulomb barrier heights as well as positions in fusion reactions the different models such as the Bass model, proximity potentials, double-folding method (DFM) and other models are used to calculate the nuclear potentials [20, 21, 28, 37, 40, 46–48]. The nucleus-nucleus potential calculated by the DFM is very sensitive to the properties of the NN effective interaction. The systematic study of the role of the parameters of the NN interaction can be found in [49, 50]. In [49], the authors compared two types of the NN effective interactions: the Reid and Paris M3Y interactions. They concluded that the calculated fusion barrier energies are generally lower than those expected, taking into account potential renormalization due to coupling to collective states at high excitation energies. The nuclear potentials calculated with the DFM using realistic M3Y interactions are much too attractive. Later, in [50], the results of the nucleus-nucleus potential calculated in the framework of the DFM by the use of the M3Y and Migdal forces. In this work [50], the authors have come to conclusions that Migdal interaction always results in the higher Coulomb barrier. The fact that the realistic M3Y interactions are too attractive has forced the authors of [51] to add the repulsion term $V_{\rm rep}\,\delta(r)$ to the effective M3Y (direct + exchange) interaction.

The use of the density-dependent Migdal forces in the DFM allows us to avoid adding the repulsion term $V_{\rm rep}$ in calculations of the capture and fusion cross sections in the dinuclear system model [4, 5, 12, 17]. In the case of collision of the intermediate and heavy mass nuclei the fusion cross section is determined not only by the Coulomb barrier but the peculiarities of the potential energy surface of the dinuclear system, which is a function of the mass and charge numbers of its fragments. The peculiarities of the potential energy surface allow us to reveal a reason for the hindrance to the complete fusion [4, 5, 12, 17]. The advance of the use of the density dependent Migdal forces is related with the fixed parameters that have been found from the description of the properties of the excited atomic nuclei [52].

Recently, the behaviors of the Coulomb barrier height is extracted from the analysis of fusion reactions, since they can provide the valuable information for the experimental exploration, especially for establishing the beam energy in synthesis of superheavy nuclei.

In the present work, we propose a method that allows us to calculate the nuclear part of the nucleus-nucleus interaction within the framework of the DFM by using an expansion of the nuclear density in Gaussian-type functions. Further, we have also calculated the theoretical values of the fusion barrier characteristics (i.e., barrier height and curvature) based on the double-folding formalism. The barrier characteristics have been used to calculate the fusion excitation function of the reactions with not-so-heavy nuclei.

This paper is organized as follows. In section 2 we present the relevant details of the proposed method based on the double-folding formalism. The expansion of the nuclear density in the Gaussian functions and the extension coefficients have been found by fitting the Fermi–Dirac distribution of nucleons. In section 3, the calculated results are compared with experimental data of the fusion barrier and with the theoretical values obtained by the large set of methods. In section 4, the calculated fusion cross sections are compared with experimental data. A brief conclusion has been given in section 5.

2. Theoretical frameworks for nucleus-nucleus potential

The results obtained by this method are compared by the nuclear part of the interaction potential between nuclei obtained by the use of the proximity potential.

The total interaction potential $V(R)$ between the projectile and target nuclei is given by

$$V(R) = V_N(R) + V_C(R) + \frac{l(l+1)\hbar^2}{2\mu R^2}, \tag{1}$$

where $V_N(R)$ is the nuclear potential; $V_C(R) = \frac{Z_1 Z_2 e^2}{R}$ represents the Coulomb potential and the last term is the centrifugal potential; $\mu = \frac{m_p m_t}{m_p + m_t}$ represents the reduced mass of the fusion system, m_p and m_t denote the masses of projectile and target nuclei in unit of $\mathrm{MeV/c^2}$, respectively; l denotes the angular momentum of the fusion system: $L = \ell\hbar$.

Once the total interaction potential $V(R)$ is calculated, the Coulomb barrier height V_B and position R_B can be extracted using the following conditions:

$$\left.\frac{dV(R)}{dR}\right|_{R=R_B} = 0, \quad \text{and} \quad \left.\frac{d^2V(R)}{dR^2}\right|_{R=R_B} \leqslant 0. \tag{2}$$

Here we calculate the Coulomb barrier parameters by adding centrifugal terms to the $l = 0$ barrier parameters.

2.1. An expansion of the nuclear density in Gaussian functions

According to the work by Münchow, Hahn, and Scheid [53] the densities of the nuclei $\rho_i(\mathbf{r})$ with $i = 1,2$ have equidensity surfaces of ellipsoidal shapes. Such a surface is given by

$$u_i^2 = \text{const}, \tag{3}$$

$$u_i^2 = \sum_{\mu=1}^{3}\sum_{\nu=1}^{3}(\delta_{\mu\nu} + \beta_{\mu\nu}^{(i)})x_\mu x_\nu/\lambda_i^2, \tag{4}$$

where $(x, y, z) = (x_1, x_2, x_3) = \mathbf{r}$. The coefficients $\beta_{\mu\nu}^{(i)}$ are the deformation parameters and λ_i are the length parameters of projectile and target nuclei. After a transformation to principal axes with coordinates x'_μ, equation (4) can be written as

$$\lambda_i^2 u_i^2 = (1 + \beta'^{(i)}_{11})x'^2_1 + (1 + \beta'^{(i)}_{22})x'^2_2 + (1 + \beta'^{(i)}_{33})x'^2_3. \tag{5}$$

Therefore, one can choose two independent deformation coordinates as dynamical variables, which may be taken as the ratios of the semi-axes of the ellipsoidal equidensity surfaces.

Then, the densities $\rho_i(\mathbf{r})$ should be expanded as follows:

$$\rho_i(\mathbf{r}) = \sum_{n=0}^{N_i} a_{in} u_i^{2n} \exp(-u_i^2), \tag{6}$$

where u_i^2 is defined in equations (4) and (5).

For the case of a spherical shapes, u_i^2 equal to r^2/λ_i^2 and then spherical densities are given according to equation (6) with $\beta'^{(i)}_{\mu\mu} = 0$:

$$\rho_i(\mathbf{r}) = \sum_{n=0}^{N_i} a_{in}\left(\frac{r}{\lambda_i}\right)^{2n} \exp\left(-\frac{r^2}{\lambda_i^2}\right), \tag{7}$$

For each nuclei, which participates in fusion reactions, the coefficients a_{in} and λ_i may be fitted with measured nuclear density distributions. Also, we can determine the exact value of λ_i under the following boundary condition:

$$\frac{R_{0i}}{\lambda_i} = 2. \tag{8}$$

Here radius R_{0i} corresponds to the radii of projectile and target nuclei has the form

$$R_{0i} = r_0 A_i^{1/3}\,\text{fm} \quad (i = 1, 2) \tag{9}$$

where r_0 is a radius parameter.

An expansion of the nuclear densities $\rho_i(\mathbf{r})$ in the Gaussian functions, we can write equation (7) as a simplified form

$$\rho_i(\mathbf{r}) = \frac{e^{-r^2/\lambda_i^2}(\lambda_i^8 a_{i0} + r^2\lambda_i^6 a_{i1} + r^4\lambda_i^4 a_{i2} + r^6\lambda_i^2 a_{i3} + r^8 a_{i4})}{\lambda_i^8}. \tag{10}$$

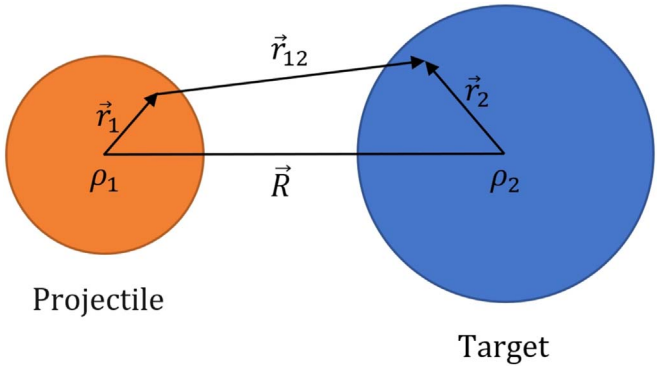

Figure 1. Schematic representation of two interacting nuclei. Coordinates of the nuclei used in the double-folding calculations.

2.2. Comparison of density distributions

The two-parameter (a and R_{0i}) Fermi–Dirac distribution

$$\rho_i(r) = \frac{\rho_{00}}{1 + \exp\left[\frac{(r - R_{0i})}{a}\right]}, \tag{11}$$

is one of the simplest models for a realistic description of the nucleon distribution in the interacting nuclei (see figure 1) and at the same time provides considerable flexibility in the analysis.

The resulting expansion coefficients a_{in} and λ_i for each nucleus are listed in table 1. The values of λ_i obtained from equation (8) are used in equation (7) to determine the density distribution and then we can determine self-consistently of density distribution coefficients a_{in} from the following equation as

$$\sum_{n=0}^{N_i} a_{in}\left(\frac{r}{\lambda_i}\right)^{2n} \exp\left(-\frac{r^2}{\lambda_i^2}\right) = \frac{\rho_{00}}{1 + \exp\left[\frac{(r - R_{0i})}{a}\right]}. \tag{12}$$

The use of the obtained expansion coefficients allows us to describe the nuclear density taken as the Fermi–Dirac distribution by the Gaussian expansion (7) for a number of nuclei with $N_i = 4$ as shown in figure 2.

It is seen from figure 2 that 5 terms in the expansion (7) are sufficient to reproduce the Fermi–Dirac distribution of numerous nuclei reasonably well.

2.3. Double-folding approach

The nuclear potential between the projectile and target nuclei is calculated by the folding of the strength of the NN interaction $v_{NN}(\mathbf{r}_{12})$ and nucleon densities of interacting nuclei as follows:

$$V_N(R) = \int d\mathbf{r}_1 \int d\mathbf{r}_2 \rho_1(\mathbf{r}_1) v_{NN}(\mathbf{r}_{12}) \rho_2(\mathbf{r}_2). \tag{13}$$

We prefer to use nucleon-nucleon potential in the form of the zero-range density-dependent potential proposed by Migdal, which is well known in his theory of finite Fermi systems [52]:

Table 1. The obtained values of the expansion coefficients a_i and λ_i for a some nuclei. The second column denotes the length parameter of nuclei.

Nuclear	λ	a_0	a_1	a_2	a_3	a_4
^{12}C	1.26	0.163 51	0.194 86	−0.015 71	0.080 25	−0.003 02
^{16}O	1.39	0.163 51	0.200 62	−0.016 18	0.080 48	−0.003 08
^{17}O	1.42	0.163 51	0.200 91	−0.016 64	0.080 91	−0.003 09
^{19}F	1.47	0.163 51	0.201 36	−0.016 81	0.081 50	−0.003 41
^{28}Si	1.68	0.163 51	0.204 12	−0.018 62	0.083 91	−0.003 85
^{32}S	1.75	0.163 51	0.205 01	−0.019 02	0.085 12	−0.003 97
^{34}S	1.79	0.163 51	0.205 64	−0.019 64	0.086 23	−0.004 03
^{35}Cl	1.81	0.163 51	0.205 72	−0.019 71	0.086 88	−0.004 11
^{36}S	1.82	0.163 51	0.205 81	−0.019 79	0.086 96	−0.004 18
^{40}Ca	1.89	0.163 51	0.211 54	−0.021 16	0.088 65	−0.004 29
^{48}Ca	1.94	0.163 51	0.215 24	−0.021 79	0.090 24	−0.004 42
^{54}Cr	2.02	0.163 51	0.217 17	−0.035 73	0.092 18	−0.004 78
^{56}Fe	2.04	0.163 51	0.217 95	−0.040 18	0.098 23	−0.004 86
^{58}Fe	2.06	0.163 51	0.218 02	−0.040 35	0.099 51	−0.005 28
^{58}Ni	2.06	0.163 51	0.218 02	−0.040 35	0.099 51	−0.005 28
^{64}Ni	2.13	0.163 51	0.220 43	−0.060 45	0.113 19	−0.007 72
^{70}Zn	2.20	0.163 51	0.220 84	−0.061 22	0.114 45	−0.007 95
^{78}Kr	2.28	0.163 51	0.223 68	−0.062 37	0.114 51	−0.008 02
^{86}Kr	2.35	0.163 51	0.224 43	−0.062 65	0.114 68	−0.008 41
^{89}Y	2.38	0.163 51	0.225 43	−0.063 22	0.116 41	−0.008 45
^{90}Zr	2.39	0.163 51	0.225 51	−0.063 53	0.116 58	−0.008 51
^{92}Zr	2.40	0.163 51	0.225 34	−0.065 73	0.120 11	−0.008 62
^{94}Sr	2.42	0.163 51	0.225 48	−0.065 89	0.120 24	−0.008 69
^{96}Zr	2.44	0.163 51	0.225 59	−0.065 98	0.120 43	−0.008 73
^{100}Zr	2.48	0.163 51	0.225 68	−0.066 11	0.120 51	−0.008 75
^{104}Mo	2.50	0.163 51	0.225 85	−0.066 89	0.120 95	−0.008 78
^{124}Sn	2.66	0.163 51	0.226 13	−0.067 11	0.122 48	−0.008 87
^{131}Sn	2.71	0.163 51	0.226 45	−0.067 75	0.123 81	−0.009 04
^{144}Sm	2.80	0.163 51	0.226 86	−0.068 17	0.125 62	−0.009 29
^{148}Sm	2.82	0.163 51	0.226 91	−0.068 33	0.125 69	−0.009 41
^{166}Er	2.93	0.163 51	0.227 34	−0.070 21	0.127 14	−0.009 54
^{197}Au	3.10	0.163 51	0.227 55	−0.071 19	0.129 41	−0.009 83
^{198}Pt	3.11	0.163 51	0.227 61	−0.071 25	0.129 50	−0.009 88
^{204}Pb	3.14	0.163 51	0.228 20	−0.071 47	0.130 36	−0.010 15
^{208}Pb	3.16	0.163 51	0.228 43	−0.072 86	0.132 02	−0.010 48
^{233}Am	3.28	0.163 51	0.228 87	−0.073 41	0.132 64	−0.011 32
^{238}U	3.30	0.163 51	0.229 30	−0.074 06	0.134 19	−0.011 53
^{248}Cm	3.35	0.163 51	0.231 06	−0.074 94	0.136 38	−0.011 95

$$v_{NN}(\mathbf{r}_1, \mathbf{r}_2) = C\left(F_{\rm ex} + (F_{\rm in} - F_{\rm ex})\frac{\rho_1(\mathbf{r}_1) + \rho_2(\mathbf{r}_2)}{\rho_{00}}\right)\delta(\mathbf{r}_{12}), \tag{14}$$

where $F_{\rm ex(in)} = f_{\rm ex(in)} \pm f'_{\rm ex(in)}$, ρ_1 and ρ_2 are densities of the projectile and target nuclei, respectively. The fixed value of the constant $C = 300\,\text{MeV fm}^3$ and the following values of the dimensionless parameters $f_{\rm in} = 0.09$; $f_{\rm ex} = -2.59$; $f'_{\rm in} = 0.42$; $f'_{\rm ex} = 0.54$ are known from the description of a large set of experimental data within the theory of finite Fermi systems [52]. The potential (14) is defined by the external amplitude ($F_{\rm ex}$), responsible for the

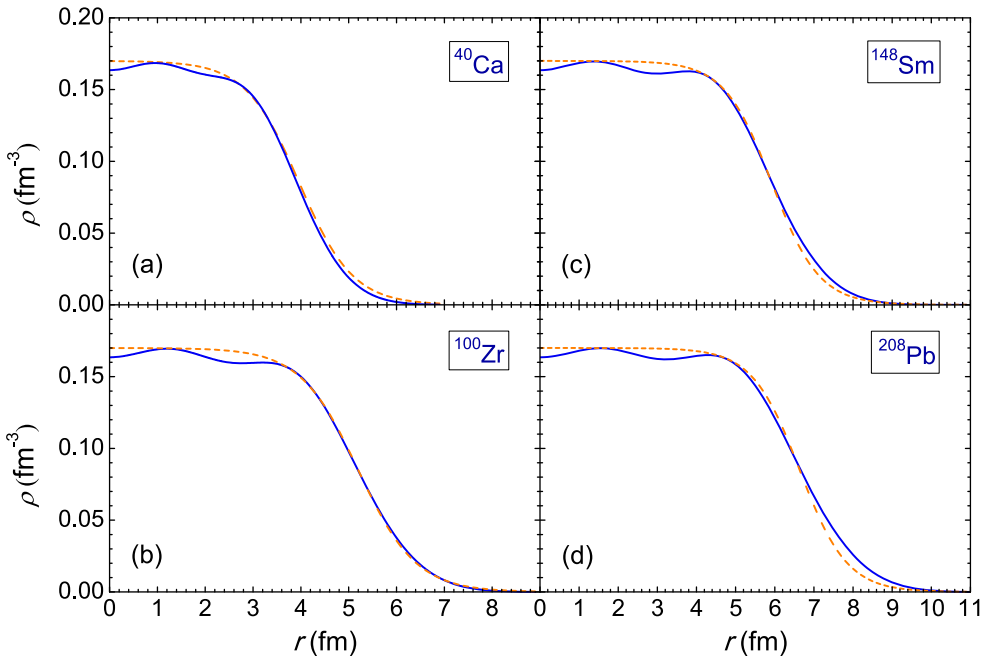

Figure 2. The spherical radial density distribution of few nuclei. The dashed line is the Fermi–Dirac distribution. The full line is the Gaussian expansion according to equation (7) using the expansion coefficients which are corresponded in table 1.

interaction of nucleons from the tails of the nuclear density distributions; by the internal amplitude ($F_{\rm in}$), responsible for the nucleon-nucleon interaction inside the nucleus. Hence, inserting the components of the Migdal potential (14) and equation (7) into double-folding integral (4), we can obtain the nuclear part of the total interaction potential as follows:

$$V_N(R) = C\Bigg[F_{\rm ex}\int \rho_1(\mathbf{r})\rho_2(\mathbf{r}-\mathbf{R})d\mathbf{r} + \frac{F_{\rm in}-F_{\rm ex}}{\rho_{00}}\Bigg(\int \rho_1^2(\mathbf{r})\rho_2(\mathbf{r}-\mathbf{R})d\mathbf{r} + \int \rho_1(\mathbf{r})\rho_2^2(\mathbf{r}-\mathbf{R})d\mathbf{r}\Bigg)\Bigg], \tag{15}$$

$$F_{\rm ex(in)} = f_{\rm ex(in)} \pm f'_{\rm ex(in)}\frac{N_1-Z_1}{A_1}\frac{N_2-Z_2}{A_2},$$

where N_i, Z_i and A_i are neutron, proton, and mass numbers of the nuclei, respectively.

In equation (15) an expanded form of $\rho_2(\mathbf{r}-\mathbf{R})$ in the Gaussian functions we can write as

$$\rho_2(\mathbf{r}-\mathbf{R}) = \exp\left(-\frac{(r^2+R^2-2rR\cos\theta)}{\lambda_2^2}\right)\Bigg[a_{20} + \frac{(r^2+R^2-2rR\cos\theta)a_{21}}{\lambda_2^2} + \frac{(r^2+R^2-2rR\cos\theta)^2 a_{22}}{\lambda_2^4} + \frac{(r^2+R^2-2rR\cos\theta)^3 a_{23}}{\lambda_2^6} + \frac{(r^2+R^2-2rR\cos\theta)^4 a_{24}}{\lambda_2^8}\Bigg], \tag{16}$$

where $|\mathbf{r} - \mathbf{R}| = \sqrt{r^2 + R^2 - 2rR\cos\theta}$, $\mathbf{R}$ characterizes the magnitude and direction of the shift of the second nuclei relative to the first one.

After inserting equations (10) and (16) into equation (15) we can numerically evaluate of the double-folding potential as follows:

$$V_N(R) = 2\pi C\Bigg[F_{\rm ex}\int_0^{\pi}\sin\theta d\theta\int_0^{\infty}\rho_1(\mathbf{r})\rho_2(\mathbf{r}-\mathbf{R})r^2dr + \frac{F_{\rm in}-F_{\rm ex}}{\rho_{00}}\Bigg(\int_0^{\pi}\sin\theta d\theta\int_0^{\infty}\rho_1^2(\mathbf{r})\rho_2(\mathbf{r}-\mathbf{R})r^2dr + \int_0^{\pi}\sin\theta d\theta\int_0^{\infty}\rho_1(\mathbf{r})\rho_2^2(\mathbf{r}-\mathbf{R})r^2dr\Bigg)\Bigg]. \quad (17)$$

Equation (17) allows the numerical evaluation of the nuclear interaction potential between two nuclei. The total interaction potential $V(R)$ is then obtained by adding the nuclear, direct plus exchange parts to the Coulomb one. As a result the Coulomb barrier heights (V_B) and positions (R_B) have been studied.

2.4. Proximity potential

The proximity potential is a well-known approach for its simplicity and numerous applications to study a variety of phenomena. All versions of proximity potential are based on the proximity force theorem. Two approaching surfaces interact with each other via force $F(s)$ due to the proximity of the surface within a small distances of $s = 2$ to 3 fm [20]. The final form of proximity potential is defined as a product of two functions. That is dependent on the shapes of two nuclei or the geometry of the nuclear system and the other is a universal function $\Phi(s)$ that only depends on the separation distance s between the half-density surfaces of the fragments.

In order to calculate the nuclear part of the total interaction potential, we use the generalized proximity potential, which is named Prox77 [20]. According to the original version of proximity potential, the interaction potential $V_N^{\rm Prox77}(r)$ between two surfaces can be written as follows

$$V_N^{\rm Prox\ 77}(r) = 4\pi\gamma b\overline{R}\Phi\left(\frac{s}{b}\right)\ \ {\rm MeV}, \quad (18)$$

where b is the surface width parameter (i.e. $b = (\pi/\sqrt{3})a$ with a=0.55 fm) and it has been taken close to 1 fm. $\overline{R}$ denotes the mean curvature radius and has the form

$$\overline{R} = \frac{C_1C_2}{C_1 + C_2}. \quad (19)$$

Here C_i are the Süssmann central radius [54, 55] of the target and projectile, and it is related to the effective sharp radius R_i as,

$$C_i = R_i\left[1 - \left(\frac{b}{R_i}\right)^2 + ...\right]\ \ (i = 1, 2). \quad (20)$$

R_i is given by the semi-empirical formula as a function of the mass number A_i,

$$R_i = 1.28A_i^{1/3} - 0.76 + 0.8A_i^{-1/3}\ \ {\rm fm}\ \ (i = 1, 2). \quad (21)$$

In equation (18), the separation distance between the half-density surfaces of two colliding nuclei s is

$$s = r - C_1 - C_2. \tag{22}$$

The surface energy coefficient γ in (18) is defined as a function of the neutron/proton excess as follows

$$\gamma = \gamma_0[1 - k_s A_s] \quad \text{MeV/fm}^2, \tag{23}$$

where A_s is the asymmetry parameter for the compound nucleus, which means drastic reduction in the magnitude of the potential with asymmetry of the colliding pair. It can be defined as

$$A_s = \frac{(N_1 + N_2) - (Z_1 + Z_2)}{A_1 + A_2}, \tag{24}$$

where Z_i and N_i are the proton and neutron numbers of target/projectile nuclei, respectively. γ_0 and k_s are 0.951 7 MeV fm^{-2} and 1.782 6, respectively.

For the original version of the proximity potential, the universal function $\Phi(\xi)$ is given by the following parametrized form [20]:

$$\Phi(\xi) = \begin{cases} -\frac{1}{2}(\xi - 2.54)^2 - 0.085\,2(\xi - 2.54)^3, \\ \qquad\qquad \text{for} \quad \xi \leqslant 1.251\,1, \\ -3.437\exp(-\xi/0.75), \\ \qquad\qquad \text{for} \quad \xi \geqslant 1.251\,1. \end{cases} \tag{25}$$

Using the above form, one can calculate the nuclear part of the interaction potential $V_N^{\text{Prox}\,77}(r)$. Based on the proximity concept, many other potentials have also been shown in the literature. In the present work, for comparative study of the Coulomb barrier heights we use different proximity-type potentials, labeled here as Proximity 1977 (Prox77) [20], Bass 1973 (RB73) [36], Christensen and Wither 1976 (CW76) [39], Broglia and Winther 1991 (BW91) [23], Aage Winther (AW95) [42], Denisov potential (DP) [56] and Ngô 1980 (Ng80) [57].

3. Results and discussion

It is seen from figure 2 that the Gaussian expansion approach allows us to reproduce well the Fermi distribution of the nucleon density of nuclei ^{40}Ca, ^{100}Zr, ^{148}Sm and ^{208}Pb. Table 1 shows the values of the expansion coefficients a_i ($i = 0, \ldots, 4$) which have been used to obtain good agreement between the approximated density and Fermi distributions of the nuclei listed there.

The nuclear part of the nucleus-nucleus interaction has been calculated for the ^{16}O+^{58}Ni, ^{40}Ca+^{86}Kr, ^{28}Si+^{166}Er and ^{36}Si+^{208}Pb reactions in the frameworks of the double-folding method by the use of the approximated density functions and of the method the proximity potential $V_N^{(\text{Prox.}77)}(r)$ to see similarities and differences in the results obtained by these methods.

In panels (a)–(d) of figure 3, the results obtained by these two methods have been compared. The difference between the nucleus-nucleus potentials calculated by the double-folding and proximity methods decreases when the Coulomb repulsion is included (at $L = 0\hbar$) that is seen from comparison of the corresponding solid and dot-dashed lines in figure 4 where the results are presented for the ^{32}S+^{40}Ca (panel a), ^{28}Si+^{166}Er (b) ^{40}Ca+^{78}Kr (c), and ^{48}Ti+^{208}Pb (d) reactions. This phenomenon is related with the difference in the positions of the minimum of the potential wells.

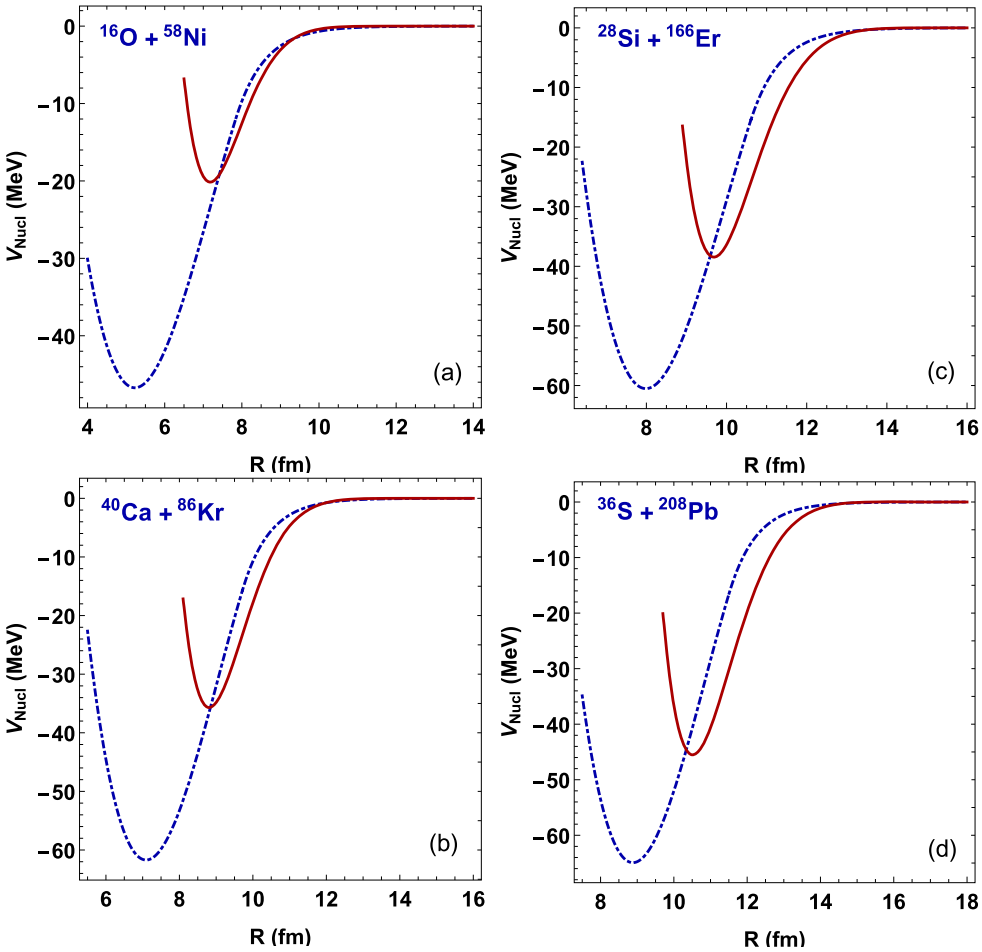

Figure 3. Comparison of the nuclear part of the interaction potential $V_{Nucl}(R)$ calculated through the proposed method in the framework of the double-folding method using density-dependent NN interaction based on Migdal forces (solid line) and the proximity potential (dot-dashed line) as a function of internuclear distance R for the four reactions shown in the corresponding panels.

In figure 5, the results of calculation by the DFM with the including the rotational energy to the nucleus-nucleus potential are presented as a function of the relative distance between interacting nuclei for the ^{36}S+^{238}U and ^{64}Ni+^{208}Pb reactions for the orbital angular momentum $L = 0$, 30, 60 and 90 $\hbar$.

The theoretical results of the Coulomb barrier V_B calculated by the present DFM potential and different types of the proximity potential for some selected fusion reactions are compared with experimental data in table 2. To make easy comparison of the results obtained by different methods with the experimental Coulomb barrier heights we present in figure 6 the deviations $\Delta V_B = V_B^{(i)} - V_B^{(\exp)}$ of those theoretical results from its values $V_B^{(\exp)}$ extracted from the analysis of the experimental data. It is seen from figure 6 that the barrier heights (full squares) found by the present double-folding potential are enough close to the values of the Coulomb barrier heights extracted from the experimental data. The deviation of the results calculated by the DFM does not exceed 2.3 MeV (maximal deviation in the comparison with

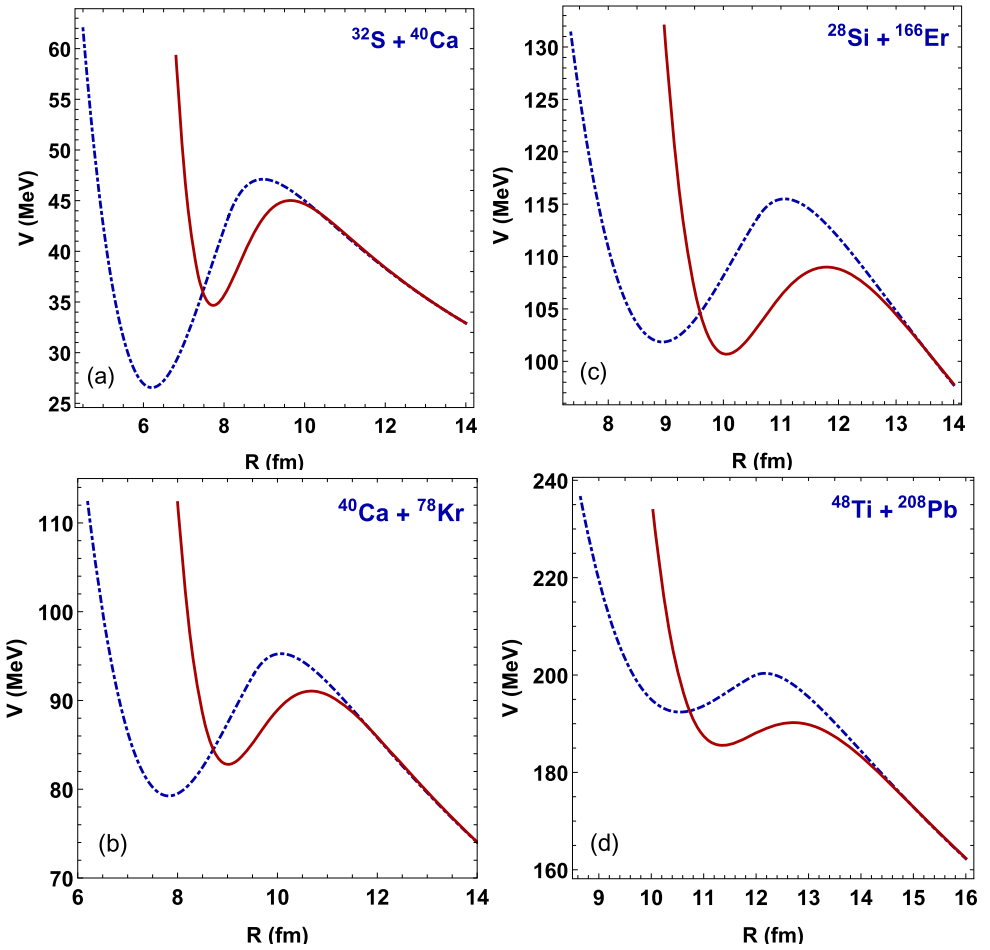

Figure 4. Comparison of the total interaction potential $V(R)$ calculated using the proposed method in the framework of the double-folding method (full line) and proximity potential (dot-dashed line) as a function of the internuclear distance R for some reactions.

^{40}Ca+^{40}Ca reaction). We can note that the versions CW76 and BW91 of the proximity potential presented in [39] and [23], respectively, allow us to obtain the results which relatively close to the experimental values of V_B: the deviation ΔV_B does not exceed 3 MeV for all reactions presented in table 2. The proximity potential used in [42] (AW95) and [20] Prox77 give deviation more than 4MeV from the experimental values of V_B for several fusion reactions. Moreover, the difference increases for the reactions with massive nuclei including the case of the last two versions and the RB73 version [36] of the proximity potential. In the region of light fusion reactions, the results of AW95 are almost identical to those of RB73. For some fusion systems, the results of BW91 are close to the experimental data, also CW76 and the present double-folding potential are close to each other. The results of DP [56] are close to the ones of AW95, and the results of RB73, Ng80, Prox77, AW95, DP are far from the experimental data, particularly, for the reactions with the massive nuclei. In the case of the ^{86}Kr+^{208}Pb reaction, the DFM with the Migdal forces better describe the experimental value of V_B than the methods BW91 and CW76 since they sufficiently underestimate the Coulomb

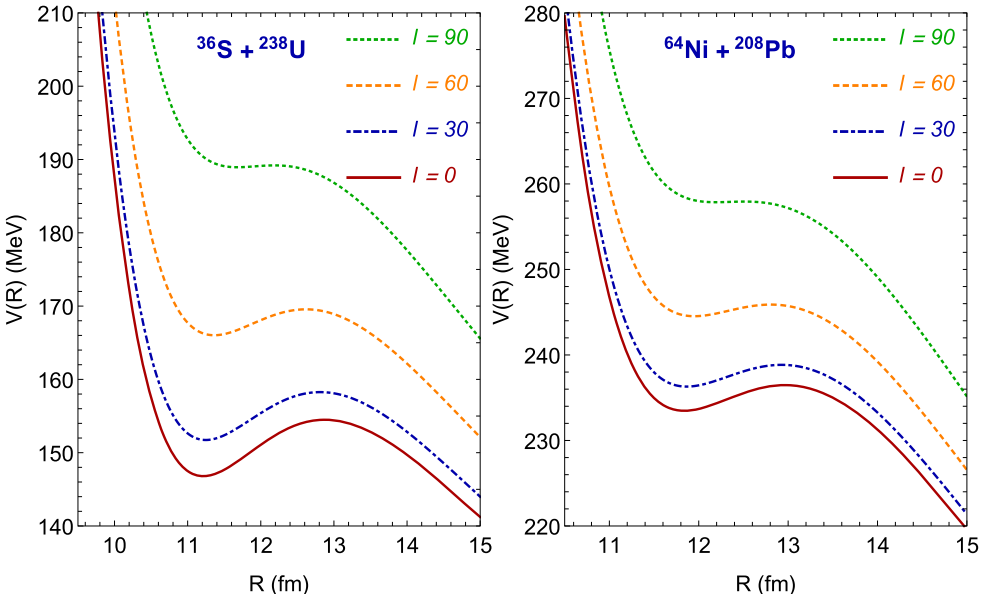

Figure 5. Comparison of the total interaction potential $V(R)$ calculated for the set of the angular momentum l values using the proposed method in the framework of the double-folding method.

barrier. In table 3, the theoretical results for the Coulomb barrier heights V_B calculated by the DFM using M3YReid interaction with zero-range exchange part and the Paris CDM3Y3 interaction with finite-range exchange part are compared with the ones calculated in this work by the Migdal interaction and experimental data obtained from the cited references.

4. The capture cross section

The knowledge of the barrier height allows us to calculate the capture cross section that contains the entrance channel effects. The capture cross section is an observable quantity and it is an interest of experimentalists and theorists studying the reaction mechanism in heavy ion collisions since only full momentum transfer to the intrinsic and collective degrees of freedom from the relative motion leads to capture [17, 71]. Its value is important to estimate the fusion probability $P_{\rm CN}$, when there is a hindrance to complete fusion: $P_{\rm CN} < 1$. This phenomenon takes place in the case of collision massive nuclei or in the collision of the two intermediate mass nuclei. The formation of a dinuclear system gives the start to complete fusion, incomplete fusion, quasifission and fast fission processes [17, 71] which are in mutual competition. Contributions of these processes to the capture cross section depends on the initial mass and charge numbers of the colliding nuclei, orbital angular momentum L and energy $E_{\rm c.m.}$ of collision. In this work we are restricted by calculations of the capture cross section for the light system or very mass-asymmetric reactions since the experimental value of the capture cross sections were measured relatively unambiguously since the capture and complete fusion cross sections are nearly equal. It means that the hindrance to complete fusion small after formation of the dinuclear system. Nevertheless in the ^{40}Ca+^{96}Zr and ^{48}Ca+^{208}Pb reactions the hindrance to complete fusion seems to be presented. This circumstance will be discussed later.

Table 2. Comparison of the Coulomb barrier heights (second column) $V_B^{(\mathrm{exp})}$ (unit is MeV) with the theoretical results V_B^{DFM} calculated by the DFM (third column) using density-dependent NN interaction with Migdal forces and by the proximity potentials for some selected fusion reactions. The results of the different types of proximity potentials corresponding to CW76 (fourth column), AW95 (fifth column), BW91 (sixth column), DP (seventh column), RB73 (eighth column), Prox77 (ninth column) and Ng80 (tenth column), respectively. The eleventh column shows the corresponding references to the sources of the experimental data.

Reaction	$V_B^{(\mathrm{exp})}$	V_B^{DFM}	V_B^{CW76}	V_B^{AW95}	V_B^{BW91}	V_B^{DP}	V_B^{RB73}	V_B^{Prox77}	V_B^{Ng80}	Refs.
^{16}O + ^{40} Ca	23.1	24.5	23.7	23.7	23.8	23.9	21.3	24.9	25.0	[35]
^{12}C + ^{92} Zr	32.3	33.5	32.3	32.5	32.5	32.4	30.2	33.9	34.1	[58]
^{16}O + ^{92} Zr	42.0	43.5	42.1	42.6	42.4	42.7	40.6	44.3	44.6	[58]
^{40}Ca + ^{48} Ca	52.0	52.5	52.6	53.6	53.0	53.8	51.7	54.2	55.8	[59]
^{40}Ca + ^{40} Ca	52.1	54.4	54.3	55.3	54.8	55.6	53.5	57.4	57.7	[35]
^{12}C + ^{204} Pb	57.6	57.9	57.9	58.8	58.3	58.0	57.9	60.7	61.1	[60]
^{16}O + ^{148} Sm	59.8	61.1	60.6	61.7	61.1	61.5	60.7	63.6	64.2	[1]
^{17}O + ^{144} Sm	60.6	60.8	60.5	61.6	61.0	61.5	60.6	63.6	64.1	[1]
^{16}O + ^{144} Sm	61.0	61.4	61.0	62.0	61.5	61.9	61.1	64.2	64.6	[1]
^{28}Si + ^{92} Zr	70.9	71.8	70.5	72.0	71.1	72.3	71.4	74.5	75.0	[58]
^{16}O + ^{208} Pb	74.5	75.3	75.5	77.0	76.1	76.5	77.2	79.4	79.8	[61]
^{36}S + ^{96} Zr	76.7	77.8	77.6	79.5	78.2	79.6	79.3	82.2	82.4	[62]
^{34}S + ^{89}Y	76.9	78.5	77.3	79.1	77.9	79.4	79.0	81.8	82.2	[63]
^{32}S + ^{89}Y	77.8	79.5	78.0	79.8	78.7	80.1	79.8	82.5	83.1	[63]
^{36}S + ^{90} Zr	78.0	79.1	78.5	80.4	79.2	80.6	80.4	83.2	83.6	[62]
^{19}F + ^{197} Au	80.8	81.1	81.5	83.3	82.1	83.0	83.9	85.7	86.2	[60]
^{35}Cl + ^{92} Zr	82.9	84.5	83.8	85.8	84.5	86.1	86.2	88.6	89.2	[58]
^{19}F + ^{208} Pb	83.0	83.5	83.8	85.6	84.4	85.3	86.4	87.9	88.5	[64]
^{40}Ca + ^{96} Zr	94.6	96.5	96.7	99.3	97.5	99.5	100.8	102.3	103.1	[65]
^{40}Ca + ^{90} Zr	96.9	98.1	97.9	100.5	98.8	100.8	102.2	103.6	104.5	[65]
^{28}Si + ^{144} Sm	104.0	102.2	102.3	105.0	103.2	105.2	107.3	108.0	109.0	[66]
^{40}Ca + ^{124} Sn	113.1	114.9	116.5	119.8	117.5	120.0	123.4	123.1	124.3	[67]
^{28}Si + ^{208} Pb	128.1	126.1	127.1	130.6	128.2	130.6	135.6	133.9	135.0	[68]
^{48}Ti + ^{208} Pb	190.1	190.2	190.1	195.3	192.4	197.0	195.4	200.3	203.1	[69]
^{54}Cr + ^{208} Pb	205.8	205.2	204.9	208.8	207.5	215.2	210.7	209.9	219.0	[69]
^{56}Fe + ^{208} Pb	223.0	222.6	221.7	228.2	224.5	230.9	228.4	233.6	237.5	[69]

Table 2. (Continued.)

Reaction	$V_B^{(\mathrm{exp})}$	V_B^{DFM}	V_B^{CW76}	V_B^{AW95}	V_B^{BW91}	V_B^{DP}	V_B^{RB73}	V_B^{Prox77}	V_B^{Ng80}	Refs.
^{64}Ni + ^{208} Pb	236.0	236.5	235.1	243.7	237.6	244.4	261.5	247.6	251.8	[69]
^{70}Zn + ^{208} Pb	250.6	250.0	249.4	258.8	252.1	259.6	278.3	262.6	267.4	[69]
^{86}Kr + ^{208} Pb	299.2	297.5	292.7	304.3	296.2	305.6	329.3	308.1	314.6	[70]

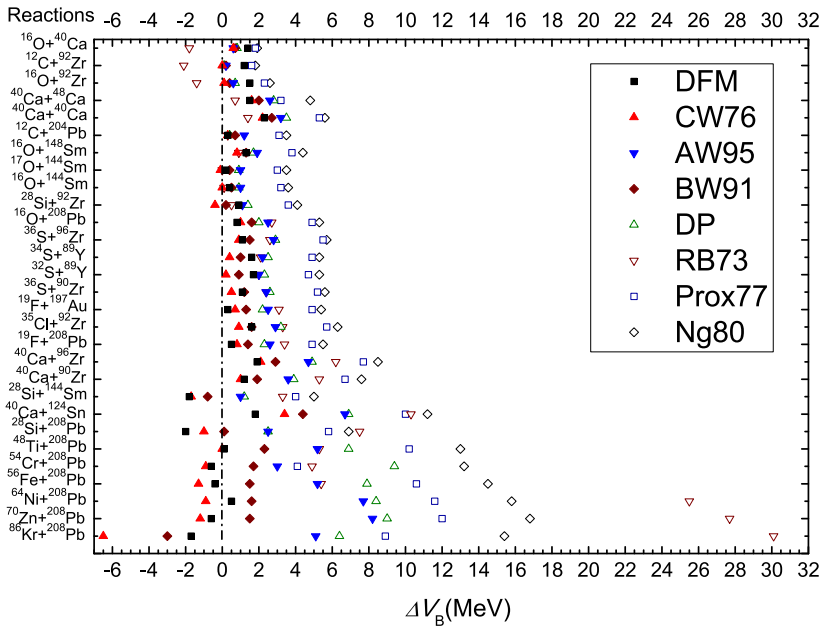

Figure 6. The deviation of the theoretical results of the Coulomb barrier V_B calculated by different methods from the experimental data obtained from the set of reactions presented on the left side of the figure. The references to the sources of the experimental data in cited papers are presented in column 11 of table 3 in this work.

The fusion cross section can be calculated by the potential energy of the entrance channel, i.e. by the nucleus-nucleus potential. To study the fusion cross sections, we will use the barrier penetration model given by Wong [72]. The fusion cross section at a given center-of-mass energy $E_{\rm c.m.}$ can be written as the sum of the cross section for each partial wave l

$$\sigma_f = \frac{\pi}{k^2}\sum_{l=0}^{l_{\max}}(2l+1)T_l(E_{\rm c.m.}), \tag{26}$$

where $k = \sqrt{\frac{2\mu E}{\hbar^2}}$ and μ is the reduced mass of the colliding nuclei. In the above fusion cross section formula, $l_{\max}$ corresponds to the largest partial wave for which a pocket still exists in the interaction potential. The interaction potential around the Coulomb barrier can be approximated by the inverted parabola. The analytical expression for the penetration probability $T_l(E_{\rm c.m.})$ is given by the well-known Hill–Wheeler formula [73]

$$T_l(E_{\rm c.m.}) = \left\{1 + \exp\left[\frac{2\pi}{\hbar\omega}(\mathrm{V_B} - \mathrm{E_{c.m.}})\right]\right\}^{-1}, \tag{27}$$

where $\hbar\omega$ is the barrier curvature. $\hbar\omega$ is related to the double derivative of the total potential at the barrier position calculated as:

$$\hbar\omega = \sqrt{-\frac{\hbar^2}{\mu}\frac{\partial^2}{\partial R^2}V(R)}\Bigg|_{R=R_B}. \tag{28}$$

If we assume that the barrier position and width are l-independent, this leads to the following fusion cross section

Table 3. Comparison of the Coulomb barrier heights (second column) $V_B^{(\exp)}$ (unit is MeV) with the theoretical results calculated by the DFM V_B^{DFM} (the third column), the DFM potential using the M3YReid interaction with zero-range exchange part ($V_B^{R\delta}$) and using the Paris CDM3Y3 interaction with finite-range exchange part (V_B^{Pf}), respectively. The results of $V_B^{R\delta}$ and V_B^{Pf} are indicated in the fourth and fifth columns, respectively.

Fusion reaction	$V_B^{(\exp)}$	V_B^{DFM}	$V_B^{R\delta}$	V_B^{Pf}	Refs.
^{16}O + ^{92} Zr	42.0	43.5	42.26	41.14	[58]
^{12}C + ^{204} Pb	57.6	57.9	58.61	57.30	[60]
^{16}O + ^{148} Sm	59.8	61.1	61.19	59.61	[1]
^{17}O + ^{144} Sm	60.6	60.8	61.10	59.53	[1]
^{16}O + ^{144} Sm	61.0	61.4	61.53	59.94	[1]
^{28}Si + ^{92} Zr	70.9	71.8	71.46	69.59	[58]
^{16}O + ^{208} Pb	74.5	75.3	77.08	75.40	[61]
^{36}S + ^{96} Zr	76.7	77.8	77.65	75.45	[62]
^{34}S + ^{89}Y	76.9	78.5	77.55	75.42	[63]
^{32}S + ^{89}Y	77.8	79.5	78.21	76.04	[63]
^{36}S + ^{90} Zr	78.0	79.1	78.26	76.01	[62]
^{19}F + ^{197} Au	80.8	81.1	83.83	81.90	[60]
^{35}Cl + ^{92} Zr	82.9	84.5	83.57	81.15	[58]
^{19}F + ^{208} Pb	83.0	83.5	85.26	83.25	[64]
^{40}Ca + ^{96} Zr	94.6	96.5	97.01	94.32	[65]
^{40}Ca + ^{90} Zr	96.9	98.1	97.78	95.01	[65]
^{28}Si + ^{144} Sm	104.0	102.2	104.37	101.72	[66]
^{40}Ca + ^{124} Sn	113.1	114.9	117.89	114.96	[67]
^{28}Si + ^{208} Pb	128.1	126.1	130.90	128.08	[68]

$$\sigma_f = \frac{10R_B^2\hbar\omega_0}{2E_{\rm c.m.}}\ln\left\{1 + \exp\left[\frac{2\pi}{\hbar\omega_l}(E_{\rm c.m.} - {\rm V_B})\right]\right\}. \tag{29}$$

In this work, we have used equation (29) to calculate the capture cross sections.

The comparison of the fusion cross section of the ^{12}C+^{204}Pb reaction calculated by equation (29) with the corresponding experimental data is presented in figure 7. One can see that the agreement with the experimental data is not so bad. The disagreement is large at the collision energies near the Coulomb barrier V_B which is reproduced well for this reaction by the DFM as seen from table 2. This fact can be explained by the use of the Fermi–Dirac distribution for the density of nucleus ^{12}C.

The agreement of the results of this work for the capture cross section with the corresponding experimental data of the ^{16}O+^{144}Sm reaction (see figure 8) is better in comparison with the ^{12}C+^{204}Pb reaction. It means that the use of the Fermi–Dirac distribution for the density of nucleus ^{16}O and more heavy nuclei is acceptable for the capture cross sections. It is seen from figure 9 that the results of the capture cross section are more close to the measured data in the case of the ^{17}O+^{144}Sm reaction. In figure 10 the theoretical and experimental results obtained for the ^{16}O+^{144}Sm and ^{17}O+^{144}Sm reactions are compared to see a role of the extra neutron in ^{17}O. Note there is a significant difference between the experimental results of these reactions and this difference has been reproduced well by the used DFM. The capture cross section calculated for the ^{19}F+^{208}Pb reaction is in good agreement with the measured data obtained from [64] (see figure 11). The conclusion is that the agreement between theoretical and experimental data improves with the increase of the

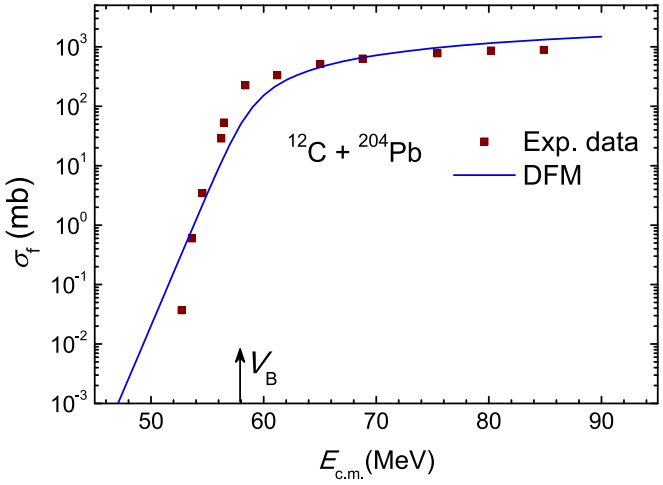

Figure 7. The comparison of the capture cross section of the ^{12}C+^{204}Pb reaction calculated by the DFM (solid line) with the corresponding experimental data (squares) obtained from [74].

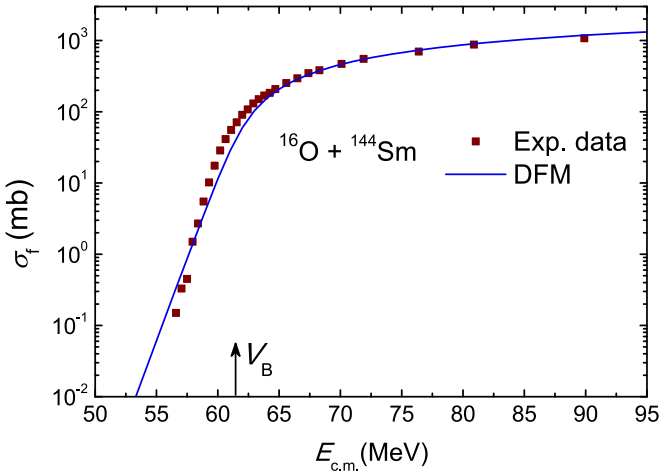

Figure 8. The comparison of the capture cross section of the ^{16}O+^{144}Sm reaction calculated by the DFM (solid line) with the corresponding experimental data (squares) obtained from [1].

mass number of the projectile nucleus in the case when light nuclei are used as a projectile. This observation is related with the fact that the application of the Fermi–Dirac distribution is favorable to describe the nucleon distribution in more heavy nuclei.

But the use of a projectile with the larger mass and charge numbers leads to appearance of the quasifission events which compete with complete fusion. This means that the complete fusion becomes smaller than capture cross section. Equation (29) describes the capture events, which is in close agreement with the complete fusion in case of the light system and/or very mass-asymmetric system. Therefore, the experimental data of the fusion cross section expects

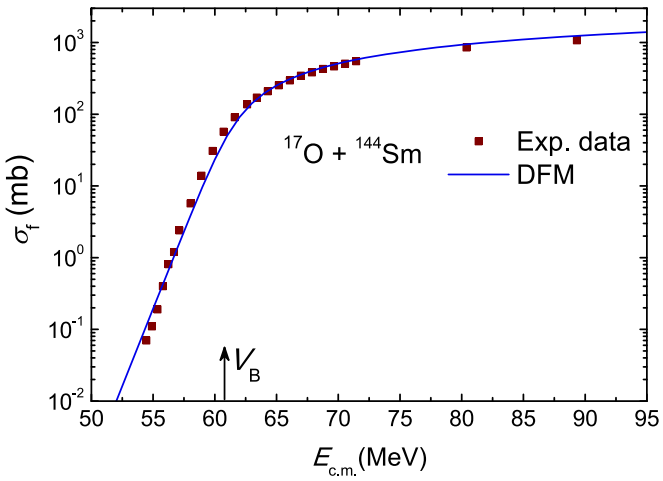

Figure 9. The comparison of the capture cross section of the ^{17}O+^{144}Sm reaction calculated by the DFM (solid line) with the corresponding experimental data (squares) obtained from [1].

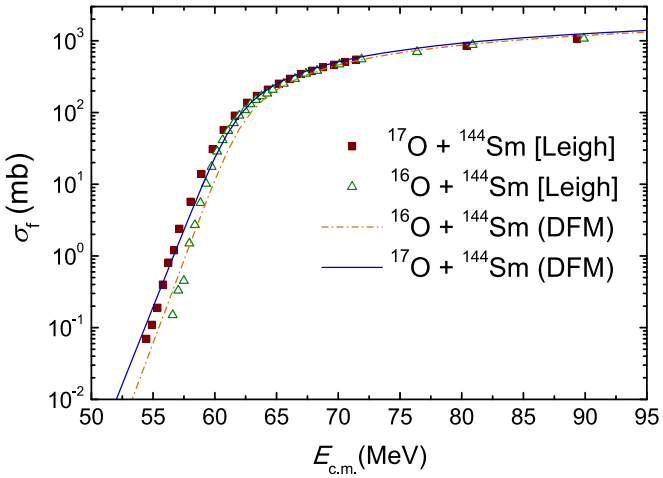

Figure 10. The comparison of the theoretical results calculated by the DFM and experimental data obtained from [1] for the ^{16}O+^{144}Sm (open triangles) and ^{17}O +^{144}Sm (full squares) reactions.

to be overestimated by equation (29) in case of the appearance hindrance to complete fusion caused by quasifission.

For example, the results of the capture cross section (thin solid line) in figure 12 obtained by the DFM for the ^{40}Ca+^{96}Zr reaction overestimate the measured data at low energies. The agreement with the experimental data can be reached taking into account the hindrance to complete fusion (thick solid line). The fusion probability estimated by the dinuclear system model [75] is less than 1 for this reaction and its values depends on energy. At lowest energies it is around $P_{\rm CN} = 0.06$. It means the fusion cross section should be obtained as a product of the capture cross section obtained by equation (29) on the fusion probability $P_{\rm CN}$. The results

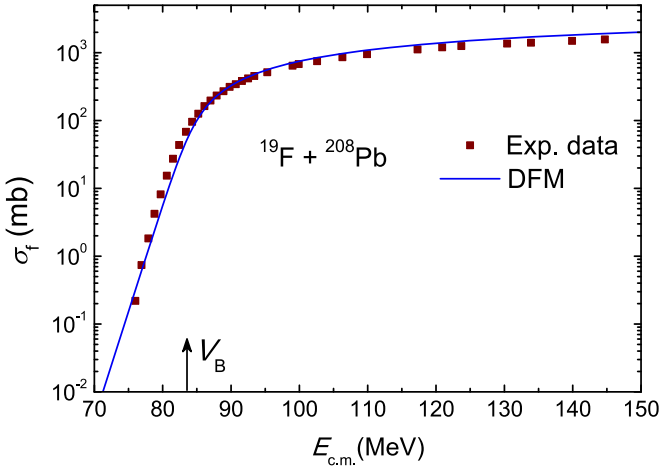

Figure 11. The comparison of the capture cross section of the ^{19}F+^{208}Pb reaction calculated by the DFM (solid line) with the corresponding experimental data (squares) obtained from [64].

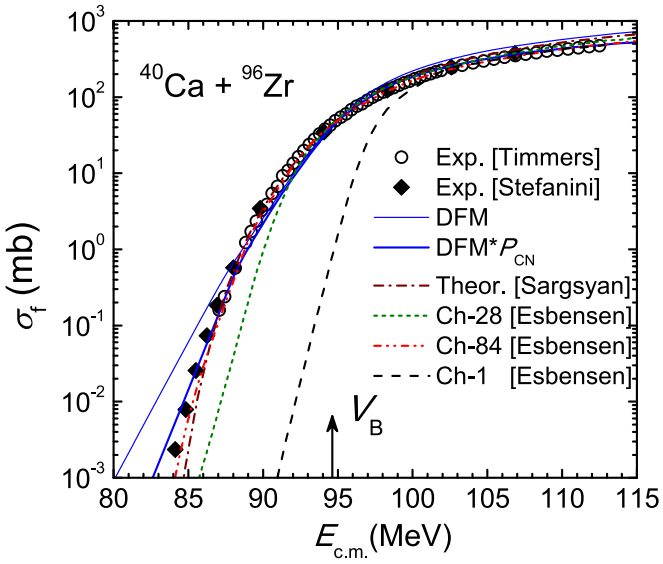

Figure 12. The comparison of the theoretical results (thin solid line-capture and thick solid line-fusion) calculated by the DFM, the ones obtained from [76] (dot-dashed line) and [51] (dot-dot-dashed line Ch-84, short-dashed line Ch-28, dashed line Ch-1) for the fusion cross section [77] of the ^{40}Ca+^{96}Zr reaction with the corresponding experimental data obtained from [65] (open circles) and from [78] (solid diamonds).

of this procedure are presented by the solid line in figure 12. This method takes into account the surface vibrations of the spherical nuclei and the possibility of the collision with the different orientations of the symmetry axis of the nuclei with a deformed shape.

Different methods have been applied to the theoretical estimation of the measured fusion data of the ^{40}Ca+^{96}Zr reaction [51, 76, 77]. The authors have included into the calculation of

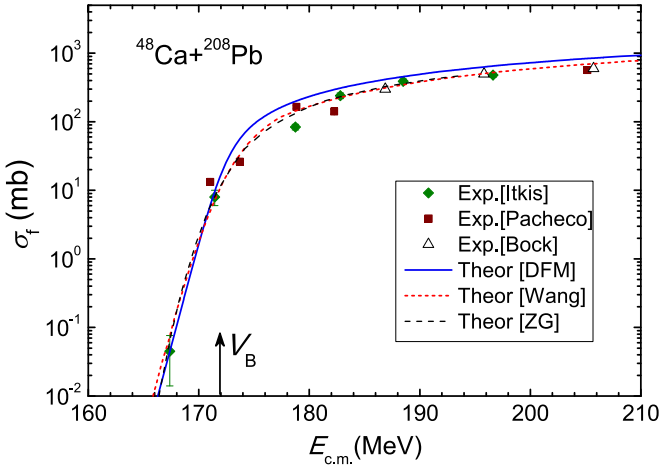

Figure 13. The comparison of the theoretical results of this work (solid line, DFM), from [79] (dotted line, WANG) and [80] (dashed line, ZG) for the fusion cross section of the ^{48}Ca+^{208}Pb reaction with the experimental data (diamonds) obtained from [81], (squares) [82], and triangles [83].

the coupling to one- and two-phonon excitations of the reacting nuclei and to one- and two-nucleon transfer effects [51, 77] to improve an agreement of the theoretical results with the measured data for this reaction. The authors of [77] have concluded the transfer strength of one and two neutrons should be taken equal to 2.25 fm and 0.355 fm, respectively, to reach good agreement with the experimental data of the ^{40}Ca+^{96}Zr reaction. These results demonstrate that the calculated fusion cross sections are sensitive not only to the pair-transfer coupling but also to the successive one nucleon transfer mechanism.

The authors of [76] have used the method of calculation including the quantum-mechanical and non-Markovian effects accompanying the passage through the potential barrier by the friction and diffusion. To reach an agreement of the results of calculation with the measured data, the authors of [76] have assumed a possibility that the two neutrons transfer from ^{96}Zr to ^{40}Ca. As a result the change of Q_{gg} causes the shift $\Delta E = 5.53$ MeV of the capture excitation function and the agreement between results of calculation and measured data has been improved very well.

The advantage of a method of calculations is in its universality to be able to reproduce the experimental data by the use as possible less free parameters and in its possibility to extract the information about physics of the reaction mechanism. From this point of view the DFM is used very widely. A single parameter is radius coefficient r_0 for calculation of the spherical radius of nuclei.

In figure 13, the experimental values of the fusion cross sections of the ^{48}Ca+^{208}Pb reaction are compared with the theoretical ones. The agreement between theoretical and experimental data is enough good for the all methods of calculation although the methods of calculations are completely different. The authors of [80] had reported the capture cross section was calculated by empirical or quantum channel coupling models (see [84]). The maximum value of angular momentum ℓ_{cr} for capture cross section was used as a free parameter together with the parameters of the proximity potential. The rich experience of the authors allowed them to suggest universal formulas (2) and (3) of the fusion probability in [80] with three adjustable parameters. At the same time the authors had noted that the formula

(3) in [80] is valid only for the cold fusion reactions of heavy nuclei with the closed shell targets ^{208}Pb and ^{209} Bi. In figure 13 the results of fusion cross section from [80] have been presented. The authors of [79] have used the Wong formula (27) as a function of the barrier heights corresponding to the deformation parameters to calculate fusion cross section and they have averaged it by the barrier distribution function $D(B)$. The method has five parameters excluding the parameters of the nucleon density functions. Important parameters is γ which allows authors to take into account the structure effects in nuclei. It changes the width of the distribution function $D(B)$. The value $\gamma = 9.5$ was used by authors of [79] to calculate the theoretical curve (dotted line) presented in figure 13.

The experimental values of the fusion cross section of the ^{48}Ca+^{208}Pb reaction were deduced from the analysis of the yields of mass symmetric binary products registered in coincidence by two detectors. The amount of the quasifission products mixed into fission products depends on the border of the frame including the mass distribution of the binary products taken around mass symmetry point $(M_1 + M_2)/2 \pm \Delta M$ at the analysis. The fusion cross sections of the experiments in [81] (solid diamonds) were deduced from the mass-energy distributions of the fission-like products while the authors of [83] (triangles) and [82] (solid squares) had used mass-angle distributions of the fission-like products. The contribution of the quasifission products, which are concentrated around initial mass numbers of the projectile and target nuclei into the analyzed volume of events, is very small. Therefore, the deduced capture cross section is nearly equal to fusion cross section. It should be noted that, in the ^{48}Ca+^{208}Pb reaction, the contribution into fusion (capture) cross sections from the yield of the evaporation residues is very small. The presence of the quasifission in this reaction was discussed in [85] in the framework of the dinuclear system model. The fusion probability was enough small and its value was obtained in the range $P_{CN} = 0.05 - 0.1$ indicating the strong hindrance to the complete fusion in the framework of the dinuclear system model.

This reaction has been considered in the recent experiments of the Australian group [86]. The problem of the extraction of the quasifission events from fusion-fission and deep-inelastic events are very actual and very important to clarify the reaction mechanisms in heavy ion collisions (see [85, 87]).

5. Conclusion

The double-folding method by the use of the expansion of the nuclear density in the Gaussian-type functions and polynomials can give the reasonable values for the Coulomb barrier heights due to the calculation of the nucleus-nucleus potential. The deviation $\Delta V_B = V_B^{DFM} - V_B^{(\exp)}$ of the Coulomb barrier heights calculated by the double-folding method from the values of the Coulomb barrier extracted from the analysis of the experimental barrier distributions for the 29 reactions does not exceed 2.3 MeV for all reactions presented in table 2.

The versions CW76 and BW91 of the proximity potential presented in [39] and [23], respectively, allow us to obtain the results which are relatively close to the experimental values of $V_B^{(\exp)}$: the deviation ΔV_B does not exceed 3 MeV for all reactions presented in table 2. The proximity potential used in [42] (AW95) and [20] Prox77 give results that deviate more than 4MeV from the experimental values of V_B for several fusion reactions. The deviation of the theoretical results of the Coulomb barrier from the experimental values increases with the increase of the mass numbers for the reactions with massive nuclei. In the region of light fusion reactions, the results of AW95 are almost identical to those of RB73. For some fusion systems, the results of BW91 [23] are close to the experimental data, also

CW76 [39] and the present double-folding potential are close to each other. The results of DP [56] are close to the ones of AW95 [42], and the results of Ng80 [57] are far from the experimental data particularly for the reactions with massive nuclei. In the case of the ^{86}Kr+^{208}Pb reaction, the double-folding method describes better the experimental value of V_B than the methods BW91 and CW76 since they sufficiently underestimate the Coulomb barrier.

The capture cross section calculated for the reaction ^{12}C+^{204}Pb with the light projectile-nucleus is in a good agreement with experimental values but it is worse than in reactions with more heavy projectiles ^{16}O and ^{19}F.

The theoretical and experimental results obtained for the ^{16}O+^{144}Sm and ^{17}O+^{144}Sm reactions are compared to see a role of the extra neutron in ^{17}O. Note there is a significant difference between the experimental results of these reactions and this difference has been reproduced well by the used DFM.

But the increase of the mass and charge numbers of a projectile-nucleus in the reaction on the same target-nucleus leads to the appearance of the quasifission events which compete with complete fusion. As a result the probability of the compound nucleus formation is reduced. For example, the agreement with the experimental data obtained for the ^{40}Ca+^{96}Zr reaction can be reached taking into account the hindrance to complete fusion. The fusion cross sections calculated by equation (29) has overestimated the measured data at low energies. Our estimation of the fusion probability by the dinuclear system model [75] showed that it is less than 1 for this reaction and its values depends on energy. At lowest energies it is around $P_{\rm CN} = 0.06$. So, the fusion cross section should be obtained as a product of the capture cross section obtained by equation (29) on the fusion probability $P_{\rm CN}$. Therefore, the experimental data of the fusion cross section expects to be overestimated by equation (29) in case of the appearance hindrance to complete fusion caused by quasifission. This is seen from figure 13 where the experimental values of the fusion cross section of the ^{48}Ca+^{208}Pb reaction are compared with the theoretical ones. The fusion experimental data does not contain quasi-fission and, therefore, this data has been described well as pure fusion cross section by the theoretical models [79, 80] and DFM used in this work. This circumstance does not mean that there is not hindrance to complete fusion in the ^{48}Ca+^{208}Pb reaction. The unambiguous establishment of the fusion probability (strength of hindrance to complete fusion) in the reaction with massive nuclei is difficult since there is a problem of identify the all capture events, i.e. the events corresponding to the full damped (full momentum transfer) reactions which are mixed with the events deep-inelastic collisions. At the same time the significant events of the quasifission events are considered as fusion-fission events (see [87]) and the hindrance to complete fusion seems to be small. The recent paper [86] is one of efforts of the experimental study of this very difficult and important problem in the analysis of the reaction mechanism in case of formation of a massive system.

Acknowledgments

The authors are grateful to Prof. Dr Werner Scheid for the suggestion to apply the approach of the expansion of the nuclear density in Gaussian-type functions in calculation of the nucleus-nucleus potential in this work and reading the manuscript. Dr. Pei Wei Wen is appreciated for reading the manuscript and useful discussions. This paper has done in the framework of the Project OT-F2-14 of the Committee for coordination science and technology development under the Cabinet of Ministers of Uzbekistan. A.K.N. thanks the Russian Foundation for Basic Research (No.17-52-45037) for the partial support.

ORCID iDs

O K Ganiev https://orcid.org/0000-0002-6812-2034
A K Nasirov https://orcid.org/0000-0002-2689-8686

References

[1] Leigh J R *et al* 1995 *Phys. Rev.* C **52** 3151–66
[2] Back B B, Esbensen H, Jiang C L and Rehm K E 2014 *Rev. Mod. Phys.* **86** 317
[3] Canto L F, Gomes P R S, Donangelo R, Lubian J and Hussein M S 2015 *Phys. Rep.* **596** 1
[4] Giardina G, Mandaglio G, Nasirov A K, Anastasi A, Curciarello F and Fazio G 2018 *Nucl. Phys.* A **970** 169
[5] Antonenko N V, Cherepanov E A, Nasirov A K, Permjakov V P and Volkov V V 1993 *Phys. Lett.* B **319** 425
[6] Dasgupta M *et al* 1999 *Phys. Rev. Lett.* **82** 1395
[7] Hong J, Adamian G G and Antonenko N V 2016 *Eur. Phys. J.* A **52** 305
[8] Diaz-Torres A, Adamian G G, Antonenko N V and Scheid W 2001 *Phys. Rev.* C **64** 024604
[9] Michel F, Reidemeister G and Ohkubo S 2002 *Phys. Rev. Lett.* **89** 152701
[10] Dasgupta M *et al* 2004 *Phys. Rev.* C **70** 024606
[11] Gomes P R S *et al* 2006 *Phys. Rev.* C **73** 064606
[12] Huang M, Zhang Z, Gan Z, Zhou X, Li J and Scheid W 2011 *Phys. Rev.* C **84** 064619
[13] Wang N, Zhao E-G, Scheid W and Zhou S-G 2012 *Phys. Rev.* C **85** 041601
[14] Zhang N T *et al* 2014 *Phys. Rev.* C **90** 024621
[15] Banerjee T, Nath S and Pal S 2015 *Phys. Rev.* C **91** 034619
[16] Fang Y D *et al* 2015 *Phys. Rev.* C **91** 014608
[17] Nasirov A, Kayumov B and Oh Y 2016 *Nucl. Phys.* A **946** 89
[18] Esbensen H 2010 *Phys. Rev.* C **81** 034606
[19] Kharab R, Chahal R and Kumar R 2016 *Nucl. Phys.* A **946** 1
[20] Blocki J, Randrup J, Świątecki W J and Tsang C F 1977 *Ann. Phys. (NY)* **105** 427
[21] Myers W D and Świątecki W J 2000 *Phys. Rev.* C **62** 044610
[22] Bass R 1980 *Lect. Notes Phys.* vol 117 (Berlin: Springer) 281
[23] Broglia R A and Winther A 1991 *Heavy Ion Reactions, Parts I and II, Frontiers in Physics* vol 84 (Redwood City, CA: Addison-Wesley)
[24] Dobrowolski A, Pomorski K and Bartel J 2003 *Nucl. Phys.* A **729** 713
[25] Mişicu Ş and Esbensen H 2006 *Phys. Rev. Lett.* **96** 112701
[26] Adaiman G G, Antonenko N V, Jolos R V, Ivanova S P, Melnikova O I *et al* 1996 *Int. Jour. Mod. Phys.* E **05** 191
[27] Denisov V Y and Noerenberg W 2002 *Eur. Phys. J.* A **15** 375
[28] Gontchar I I, Hinde D J, Dasgupta M and Newton J O 2004 *Phys. Rev.* C **69** 024610
[29] Newton J O, Butt R D, Dasgupta M, Hinde D J, Gontchar I I, Morton C R and Hagino K 2004 *Phys. Rev.* C **70** 024605
[30] Gupta Raj K, Manhas M, Münzenberg G and Greiner W 2005 *Phys. Rev.* C **72** 014607
[31] Dutt I and Puri R K 2010 *Phys. Rev.* C **81** 044615
[32] Dutt I and Puri R K 2010 *Phys. Rev.* C **81** 064608
[33] Dutt I and Puri R K 2010 *Phys. Rev.* C **81** 064609
[34] Zhang G L, Qu W W, Guo M F, Zhang H Q, Wolski R and Qian J Q 2016 *Eur. Phys. J.* A **52** 39
[35] Zhang G L and Pan M 2016 *Int. J. Mod. Phys.* E **25** 1650082
[36] Bass R 1973 *Phys. Lett.* B **47** 139
[37] Bass R 1974 *Nucl. Phys.* A **231** 45
[38] Bass R 1977 *Phys. Rev. Lett.* **39** 265
[39] Christensen P R and Winther A 1976 *Phys. Lett.* B **65** 19
[40] Reisdorf W 1994 *J. Phys. G: Nucl. Part. Phys.* **20** 1297
[41] Akyüz O and Winther A 1979 (*Proc. of the Enrico Fermi International School of Physics*) ed R A Broglia, C H Dasso and R Ricci (Amsterdam: North-Holland) 1981
[42] Winther A 1995 *Nucl. Phys.* A **594** 203

[43] Woods R D and Saxon D S 1954 *Phys. Rev.* **95** 577
[44] Ghodsi O N and Torabi F 2015 *Phys. Rev.* C **92** 064612
[45] Satchler G R and Love W G 1979 *Phys. Rep.* **55** 183
[46] Krappe H J, Nix J R and Sierk A J 1979 *Phys. Rev.* C **20** 992
[47] Adel A and Alharbi T 2017 *Eur. Phys. J.* A **53** 1
[48] Wang B, Wen K, Zhao W J, Zhao E G and Zhou S G 2017 *At. Data Nucl. Data tables* **114** 281
[49] Gontchar I I, Hinde D J, Dasgupta M and Newton J O 2004 *Phys. Rev.* C **69** 024610
[50] Gontchar I and Chushnyakova M V 2016 *J. Phys. G: Nucl. Part. Phys.* **43** 045111
[51] Esbensen H and Stefanini A M 2014 *Phys. Rev.* C **89** 044616
[52] Migdal A B 1982 *Theory of Finite Fermi Systems and Applications to the Atomic Nuclei* (Moscow: Nauka)
[53] Münchow M, Hahn D and Scheid W 1982 *Nucl. Phys.* A **388** 381
[54] Süssmann G 1973 *Lawrence Berkeley Laboratory Report* LBL-1615
[55] Myers W D 1973 *Nucl. Phys.* A **204** 465
[56] Denisov V Y 2002 *Phys. Lett.* B **526** 315
[57] Ngô H and Ngô C 1980 *Nucl. Phys.* A **348** 140
[58] Newton J O, Morton C R, Dasgupta M, Leigh J R, Mein J C, Hinde D J and Timmers H 2001 *Phys. Rev.* C **64** 064608
[59] Trotta M, Stefanini A M, Corradi L, Gadea A, Scarlassara F, Beghini S and Montagnoli G 2001 *Phys. Rev.* C **65** 011601(R)
[60] Berriman A C, Hinde D J, Dasgupta M, Morton C R, Butt R D and Newton J O 2001 *Nature (London)* **413** 144
[61] Morton C R, Berriman A C, Dasgupta M, Hinde D J, Newton J O, Hagino K and Thompson I J 1999 *Phys. Rev.* C **60** 044608
[62] Stefanini A M *et al* 2000 *Phys. Rev.* C **62** 014601
[63] Mukherjee A, Dasgupta M, Hinde D J, Hagino K, Leigh J R, Mein J C, Morton C R, Newton J O and Timmers H 2002 *Phys. Rev.* C **66** 034607
[64] Hinde D J, Berriman A C, Dasgupta M, Leigh J R, Mein J C, Morton C R and Newton J O 1999 *Phys. Rev.* C **60** 054602
[65] Timmers H, Ackermann D, Beghini S, Corradi L, He J H, Montagnoli G, Scarlassara F, Stefanini A M and Rowley N 1998 *Nucl. Phys.* A **633** 421–45
[66] Dasgupta M, Hinde D J, Leigh J R, Lemmon R C, Mein J C, Morton C R, Newton J O and Timmers H 1994 *Proc. of the Workshop on Heavy-Ion Fusion, Padova, Italy* (Singapore: World Scientific Press) 115
[67] Scarlassara F, Beghini S, Montagnoli G, Segato G F, Ackermann D, Corradi L, Lin C J, Stefanini A M and Zheng L F 2000 *Nucl. Phys.* A **672** 99
[68] Hinde D J, Morton C R, Dasgupta M, Leigh J R, Mein J C and Timmers H 1995 *Nucl. Phys.* A **592** 271
[69] Mitsuoka S, Ikezoe H, Nishio K, Tsuruta K, Jeong S C and Watanabe Y 2007 *Phys. Rev. Lett.* **99** 182701
[70] Ntshangase S S *et al* 2007 *Phys. Lett.* B **651** 27
[71] Avazbek N, Kyungil K, Giuseppe M, Giorgio G, Akhtam M and Youngman K 2013 *Eur. Phys. J.* A **49** 147
[72] Wong C Y 1973 *Phys. Rev. Lett.* **31** 766
[73] Hill D L and Wheeler J A 1953 *Phys. Rev.* **89** 1102
[74] Mukherjee A, Hinde D J, Dasgupta M, Hagino K, Newton J O and Butt R D 2007 *Phys. Rev.* C **75** 044608
[75] Kim K, Kim Y, Nasirov A K, Mandaglio G and Giardina G 2015 *Phys. Rev.* C **91** 064608
[76] Sargsyan V V, Adamian G G, Antonenko G G, Scheid W and Zhang H Q 2012 *Phys. Rev.* C **86** 034614
[77] Esbensen H, Montagnoli G and Stefanini A M 2016 *Phys. Rev.* C **93** 034609
[78] Stefanini A M *et al* 2014 *Phys. Lett.* B **728** 639–44
[79] Wang N, Wu X, Li Z, Liu M and Scheid W 2006 *Phys. Rev.* C **74** 044604
[80] Zagrebaev V and Greiner W 2008 *Phys. Rev.* C **78** 034610
[81] Itkis M G *et al* 2006 *AIP Conf. Proc.* **853** 231
[82] Pacheco A J, Fernández N J O, DiGregorio D E, di Tada M, Testoni J E, Chan Y, Chávez E, Gazes S, Plagnol E and Stokstad R G 1992 *Phys. Rev.* C **45** 2861–9

[83] Bock R *et al* 1982 *Nucl. Phys.* A **388** 334
[84] Zagrebaev V I *et al* 2001 *Phys. Rev.* C **65** 014607
[85] Fazio G *et al* 2005 *Mod. Phys. Lett.* A **20** 391
[86] Banerjee K *et al* 2019 *Phys. Rev. Lett.* **122** 232503
[87] Nasirov A K, Giardina G, Mandaglio G, Manganaro M, Hanappe F, Heinz S, Hofmann S, Muminov A I and Scheid W 2009 *Phys. Rev.* C **79** 024606